

Comparison of forcing functions in magnetohydrodynamics

Mairi E. McKay^{1,*}, Moritz F. Linkmann², Daniel Clark¹, Adam A. Chalupa¹, and Arjun Berera^{1†}

¹ *The School of Physics and Astronomy,
The University of Edinburgh, Edinburgh, Scotland and*

² *Department of Physics & INFN,
University of Rome Tor Vergata,
Via della Ricerca Scientifica 1, 00133 Rome, Italy*

(Dated: April 18, 2017)

Abstract

Results are presented of direct numerical simulations of incompressible, homogeneous magnetohydrodynamic turbulence without a mean magnetic field, subject to different kinetic forcing functions commonly used in the literature. Specifically, the forces are negative damping (which uses the large-scale field as a forcing function), a nonhelical random force, and a nonhelical static sinusoidal force (analogous to helical ABC forcing). The time evolution of the three ideal invariants (energy, magnetic helicity and cross helicity), the time-averaged energy spectra, the energy ratios and the dissipation ratios are examined. The effect of the number of grid points and Reynolds number on the performance of the forces is also considered. All three forces produce qualitatively similar steady states with some differences. In particular, the magnetic helicity is well-conserved in all cases but the sinusoidal method of energy injection has a tendency to introduce cross helicity into the system. Indeed, an ensemble of sinusoidally-forced simulations with identical parameters shows large variations in the cross helicity over long time periods, casting some doubt on the validity of the principle of ergodicity in systems where the injection of helicity cannot be controlled. Cross helicity can unexpectedly enter the system through the forcing function and must be carefully monitored.

* mairi.mckay@ed.ac.uk

† ab@ph.ed.ac.uk

I. INTRODUCTION

Turbulence is a diverse and complex phenomenon that has been a source of interest for a hundred years, if not more, and from many different disciplines. The hydrodynamic equations which describe turbulent flow are well-known but their nonlinear nature prohibits a complete understanding of them. Maxwell's equations of electromagnetism can be combined with hydrodynamics to form the magnetohydrodynamic (MHD) equations, which describe the effect of a magnetic field on a conducting fluid. These equations can be applied to many astrophysical and geophysical flows [1–4].

The advent of high performance computing has caused a rapid growth in the study of turbulence. Direct numerical simulations (DNS) are a computationally expensive tool which allows us to follow the exact evolution of a turbulent flow without introducing any modelling. However, it is often useful to inject energy into a turbulent system to compensate for the energy lost through dissipation, and in these forced simulations, a decision has to be made about the method of energy injection. Once a balance is achieved between the energy lost and the energy injected, the system's statistical properties can be studied. Homogeneous turbulence, which allows fundamental aspects of turbulence to be studied without concern for additional effects from, e.g. boundary conditions, is often simulated. Strictly speaking, an infinite computational domain is required for homogeneous turbulence but periodic boundary conditions are often used as a cheaper alternative.

A wide range of approaches to forcing homogeneous turbulence simulations has been used over the years. Most often these involve injecting energy into the smallest wavenumbers, with or without introducing some random component, eg [5–7]. Different forcing methods have different advantages. A deterministic force could be seen as more physical but stochastic forces may provide better control over energy and helicity input. Another example is that a deterministic forcing may produce longer fluctuations than a stochastic forcing and so may require a longer run-time to obtain reasonable statistics, despite being more efficient computationally [7].

At the core of the study of homogeneous isotropic turbulence are the contributions of Richardson, Kolmogorov and Obukhov, which include the energy cascade (the notion that energy is transferred from large scales to progressively smaller scales where dissipation dominates), the self-similar scaling of structure functions and the famous ‘five-thirds’ power law, $E(k) \propto k^{-5/3}$. These features give rise to the concept of universality of scaling exponents, which is the idea that the small-scale evolution of a turbulent system is independent of the large-scale features, such as geometry or the method of energy injection. These concepts have been supported by many experiments, numerical simulations and theoretical arguments since then [3, 8, 9].

The concept of universality in magnetohydrodynamics (MHD) is questionable;

highlighted especially by the unusual presence of an inverse cascade of magnetic helicity under certain conditions, which causes some energy to be transferred to the large scales [10–13]. It is known that nonzero values of magnetic helicity and cross helicity, two of the three MHD ideal invariants [14] (the third being total energy), can alter aspects of MHD systems such as the dimensionless dissipation rate [15–17]. This comes as a result of selective decay processes, that is, the tendency for the fields to self-organise into a force-free state in which the magnetic helicity is maximal, or an Alfvénic state where the velocity and magnetic fields are fully aligned [1, 18]. The alignment of the fields weakens the turbulence, slowing down the decay of energy in unforced systems [1, 19].

Interestingly, it was found that self-organised states can be obtained when both fields are forced in a nonhelical way, depending on the time-correlation of the forcing [20]. The less often the phase was randomised, the more the cross helicity and magnetic helicity would build up, leading to self-organisation. It is important to be sure that effects such as these are independent of the specific implementation of the forcing, especially since MHD has far-reaching cosmological and astrophysical applications and relies heavily on results from numerical simulations. There has been no systematic study that examines the effect of different forcing functions in MHD. The importance of understanding how independent the turbulence properties are of the forcing function has been underpinned by the above discussion. This paper, as far as we are aware, is the first to conduct such a study.

In this paper we investigate the evolution of homogeneous, incompressible MHD turbulence without a mean magnetic field, subject to three different types of kinetic forcing functions which aim to represent the range of forcing methods used in the literature. Specifically, we use: one which uses the large-scale field as a forcing function, a nonhelical random force defined by using time-varying helical basis vectors, and a nonhelical static sinusoidal force. In Sec. II we give details of our simulations, including the three forcing routines. In Sec. III we examine the time evolution of the three ideal invariants (energy, magnetic helicity and cross helicity), the time-averaged energy spectra, the energy ratios and the dissipation ratios. As we will show, the magnetic helicity is well-conserved in all cases but the sinusoidal method of energy injection has a tendency to introduce cross helicity into the system. Indeed, our results for sinusoidally-forced simulations with identical parameters and different initial conditions show large variations in the normalised cross helicity over long time periods. We show that this is not lessened by increasing the number of grid points. We discuss these results in Sec. IV and draw some conclusions.

Run ID	Type	N	ν	Re	Re_λ	k_{max}/k_η	k_{max}/k_ν	ρ_b	ρ_c	ρ_u	ϵ_b	ϵ_u
AHFa	AHF	512	0.0008	742	180	1.50	1.88	0.008	0.026	5.41×10^{-07}	0.082	0.034
NDa	ND	512	0.0008	994	213	1.56	1.96	-0.004	-0.034	0.0312	0.071	0.028
SFa	SF	512	0.0008	1190	236	1.55	1.94	-0.006	-0.156	0.00182	0.072	0.029
AHFb	AHF	512	0.001	609	162	1.77	2.20	-0.003	0.011	-6.73×10^{-6}	0.082	0.035
NDb	ND	512	0.001	803	179	1.85	2.28	-0.025	0.212	-0.00116	0.069	0.03
SFb	SF	512	0.001	940	207	1.85	2.31	0.0004	-0.012	0.000626	0.069	0.029
AHFc	AHF	256	0.0015	374	125	1.25	1.51	-0.004	-0.008	7.39×10^{-6}	0.068	0.033
NDc	ND	256	0.0015	535	152	1.25	1.53	-0.005	-0.088	0.0305	0.068	0.031
SFc	SF	256	0.0015	618	164	1.25	1.55	0.011	-0.03	-0.00335	0.069	0.029
AHFd	AHF	256	0.002	308	113	1.55	1.82	0.007	-0.007	-1.73×10^{-5}	0.068	0.036
NDd	ND	256	0.002	410	134	1.56	1.88	-0.013	0.001	0.0422	0.067	0.032
SFd	SF	256	0.002	541	161	1.45	1.76	-0.003	0.013	0.000890	0.091	0.041
AHFe	AHF	128	0.005	127	62	1.61	1.61	-0.003	-0.009	-6.30×10^{-6}	0.053	0.052
NDe	ND	128	0.005	171	76	1.58	1.72	0.002	0.024	-0.0277	0.057	0.041
SFe	SF	128	0.005	211	89	1.46	1.65	0.019	0.104	-0.0108	0.077	0.047
AHFf	AHF	128	0.008	81	45	2.37	2.17	0.012	0.002	1.46×10^{-5}	0.046	0.066
NDf	ND	128	0.008	100	51	2.49	2.23	-0.0006	-0.038	0.000274	0.038	0.059
SFf	SF	128	0.008	136	67	2.25	2.21	-0.008	0.001	-2.14×10^{-5}	0.057	0.061

TABLE I: Table of basic parameters including the forcing type, number of grid points N^3 , viscosity ν , integral-scale and Taylor-scale Reynolds numbers Re and

Re_λ respectively, resolution k_{max}/k_ν and k_{max}/k_η defined with respect to the velocity and magnetic fields, relative magnetic helicity ρ_b , relative cross helicity ρ_c , relative kinetic helicity ρ_u , and magnetic and kinetic dissipation rates ϵ_b and ϵ_u . The values were time-averaged over the duration of the steady state. AHF stands for adjustable helicity forcing, ND for negative damping, SF for sinusoidal forcing.

II. NUMERICAL METHOD

We performed direct numerical simulations of the incompressible MHD equations

$$\partial_t \mathbf{u} = -\nabla P - (\mathbf{u} \cdot \nabla) \mathbf{u} + (\nabla \times \mathbf{b}) \times \mathbf{b} + \nu \nabla^2 \mathbf{u} + \mathbf{f} \quad (1)$$

$$\partial_t \mathbf{b} = \nabla \times (\mathbf{u} \times \mathbf{b}) + \eta \nabla^2 \mathbf{b} \quad (2)$$

$$\nabla \cdot \mathbf{u} = 0, \nabla \cdot \mathbf{b} = 0, \quad (3)$$

where \mathbf{u} is the velocity field, \mathbf{b} the magnetic field in Alfvén units, P the pressure, ν the viscosity, η the magnetic diffusivity and \mathbf{f} is an external force which we will

define later. The density was set to 1. We solved these equations numerically using a pseudospectral, fully-dealiased code (see [21, 22] for details) on a three-dimensional periodic domain with lattice sizes varying from 128^3 to 512^3 points (see Table I). The simulations were all spatially well-resolved, with the maximum resolved wavenumber always at least 1.25 times greater than the Kolmogorov microscales $k_\nu = (\nu^3/\epsilon_u)^{1/4}$ and $k_\eta = (\eta^3/\epsilon_b)^{1/4}$, where ϵ_u and ϵ_b are the kinetic and magnetic dissipation rates. For simplicity we limited our study to the case where the magnetic Prandtl number, $\text{Pm} = \nu/\eta$, is one.

We examined the variations of the relative magnetic helicity and cross helicity, defined respectively as

$$\rho_b = \langle \mathbf{b} \cdot \mathbf{a} \rangle / (\langle |\mathbf{b}|^2 \rangle \langle |\mathbf{a}|^2 \rangle)^{1/2} \quad (4)$$

$$\rho_c = \langle \mathbf{u} \cdot \mathbf{b} \rangle / (\langle |\mathbf{u}|^2 \rangle \langle |\mathbf{b}|^2 \rangle)^{1/2}, \quad (5)$$

where \mathbf{a} is the magnetic vector potential, $\mathbf{b} = \nabla \times \mathbf{a}$, and the angular brackets denote a spatial average. These quantities are useful because the three ideal invariants in dissipationless MHD are magnetic helicity, cross helicity and total energy. The relative kinetic helicity is defined as

$$\rho_u = \langle \mathbf{u} \cdot \boldsymbol{\omega} \rangle / (\langle |\mathbf{u}|^2 \rangle \langle |\boldsymbol{\omega}|^2 \rangle)^{1/2}, \quad (6)$$

where $\boldsymbol{\omega} = \nabla \times \mathbf{u}$ is the vorticity.

Three types of forcing function were used: negative damping (ND), adjustable helicity forcing (AHF) and sinusoidal forcing (SF) which are defined as follows:

A. Negative damping

The negative damping function uses the large-scale velocity field as a forcing function. It was first developed as a way to avoid introducing further randomness into an already random system [23] and is commonly used in hydrodynamic simulations [16, 24–27]. The function is

$$\mathbf{f}(\mathbf{k}, t) = \begin{cases} \frac{\epsilon_i \mathbf{u}(\mathbf{k}, t)}{2E_{u, k_f}(t)}, & \text{if } 1 \leq k \leq k_f \\ 0 & \text{otherwise,} \end{cases} \quad (7)$$

where $E_{u, k_f}(t) = \int_1^{k_f} E_u(k, t) dk$ is the kinetic energy contained in the forcing range $[1, k_f]$ and ϵ_i is an adjustable parameter. The rate of energy injection is $\langle \mathbf{u} \cdot \mathbf{f} \rangle = \epsilon_i$ which will be equal to the total dissipation rate $\epsilon = \epsilon_b + \epsilon_u$ during the steady state. We chose our fields' initial conditions to have negligible kinetic, magnetic and cross helicity and therefore one might expect the fields to remain nonhelical throughout their evolution, although the actual helicity injection cannot be controlled. The variation of helicity due to negative damping was explored to some extent in [27].

The forcing type has been well-used, but nevertheless, it was recently found that, in hydrodynamics, at low Reynolds numbers, negative damping can induce self-ordering effects due to poor kinetic helicity conservation [28, 29].

B. Adjustable helicity forcing

The second type of forcing considered uses a helical basis composed of eigenvectors of the curl operator:

$$\mathbf{f}(\mathbf{k}, t) = A(\mathbf{k})\mathbf{e}_1(\mathbf{k}, t) + B(\mathbf{k})\mathbf{e}_2(\mathbf{k}, t) , \quad (8)$$

where $\mathbf{e}_1 \cdot \mathbf{e}_2^* = \mathbf{e}_1 \cdot \mathbf{k} = \mathbf{e}_2 \cdot \mathbf{k} = 0$ and \mathbf{e}_1 and \mathbf{e}_2 are unit vectors which satisfy $i\mathbf{k} \times \mathbf{e}_1 = k\mathbf{e}_1$ and $i\mathbf{k} \times \mathbf{e}_2 = -k\mathbf{e}_2$. At each forcing time step a random vector \mathbf{k} with magnitude $1 \leq k \leq k_f$ is selected. From this, a random perpendicular unit vector is generated and used to construct the helical basis. Thus the basis is changed every time the forcing function is called. $A(\mathbf{k})$ and $B(\mathbf{k})$ are complex parameters which can be adjusted to control the helicity of the forcing [30]. In our simulations we set the kinetic helicity to zero, so the forcing was explicitly nonhelical. This type of forcing has been widely used [30–34].

C. Sinusoidal forcing

The sinusoidal forcing we used is deterministic and nonhelical, implemented in real space:

$$\mathbf{f}(\mathbf{x}) = C \sum_{k=1}^{k_f} \begin{pmatrix} \sin(kz) + \sin(ky) \\ \sin(kx) + \sin(kz) \\ \sin(ky) + \sin(kx) \end{pmatrix} , \quad (9)$$

where C is an adjustable constant. This forcing type was used in Ref. [20]. It is the nonhelical analogue of the well-known ABC forcing, which is fully helical [35–37]. It is worth noting that the sinusoidal forcing is nonhelical on average over all space in the continuous limit. As such, it is possible that the discretisation of the system onto a lattice could introduce distortions.

III. RESULTS

A. Energy evolution

We will describe our results using the $\nu = 0.008$ (AHFf, Ndf, SFf) and $\nu = 0.0008$ (AHFa, NDa, SFa) simulations as our main focus, since they attained respectively the lowest and highest Reynolds numbers in our tests (see Tab. I).

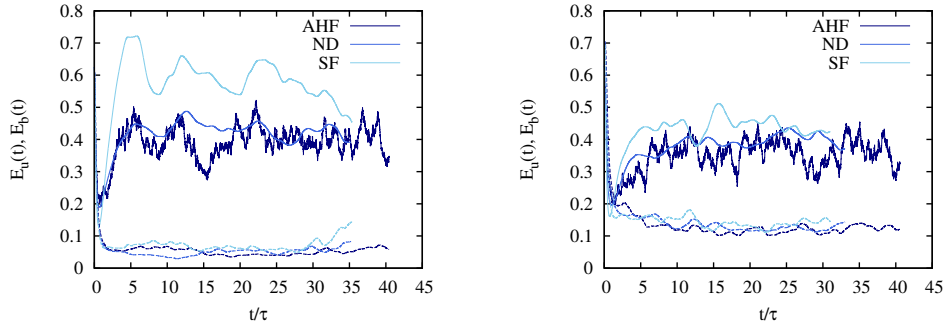


FIG. 1: Evolution of kinetic energy (solid lines) and magnetic energy (dashed lines) for runs AHFf, NDf, SFf (left) and AHFa, NDa, SFa (right). τ is the steady state large eddy turnover time.

Using these simulations, which are representative of the various other simulations we ran, we will highlight features of the three forcing functions.

We centre our analysis on various properties of the forced systems while in a statistically steady state. This allows us to look at time-averaged samples of data taken during that period. Figure 1 shows the time evolution of kinetic and magnetic energy for runs AHFf, NDf, SFf and AHFa, NDa, SFa. The steady state follows an initial transition period in which the fields evolve into a fully-developed statistically steady turbulent state, where the energy injected equals the energy dissipated. We began taking measurements after the transient initial behaviour had passed and both the kinetic and magnetic energies were fluctuating around a constant value. The AHF kinetic energy evolution, as seen in Fig. 1, is more erratic than the other two forcing types. This is due to the random nature of the forcing function, as described in Sec. II B, which causes rapid changes in the amount of energy injected. The time scale was normalised by τ , the steady state large eddy turnover time. All simulations lasted for 100 units of simulation time, corresponding to approximately 30 to 40 large eddy turnover times. The AHF runs generally had a slightly smaller value of τ , meaning that the injected energy was transferred to the smaller scales at a faster rate.

We will use either the integral-scale Reynolds number $Re = u_{rms}L/\nu$ or the Taylor-scale Reynolds number $Re_\lambda = u_{rms}\lambda/\nu$ as metrics to measure the turbulence, since the integral-scale Reynolds number is associated with the forcing scales while the Taylor-scale Reynolds number characterises the turbulence at intermediate scales. Here $L = 3\pi \int_0^\infty k^{-1}E_u(k)dk / (4 \int_0^\infty E_u(k)dk)$ is the integral-scale length, $\lambda = (15\nu/\epsilon)^{1/2}u_{rms}$ is the Taylor microscale, $E_u(k)$ is the steady state kinetic energy spectrum and u_{rms} is the root-mean-square velocity. In an isotropic system, $u_{rms}^2 = \langle u_i^2 \rangle$ for any direction i , so the total kinetic energy $E_u = 3u_{rms}^2/2$.

Two-dimensional slices of the fields from the AHFa, NDa and SFa simulations at a point in time during the steady state are shown in Fig. 2. These slices are

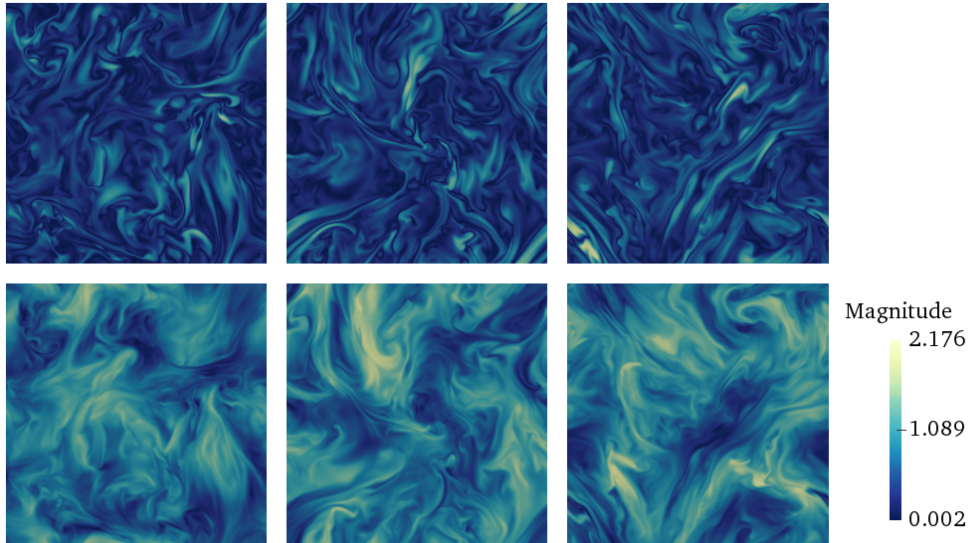


FIG. 2: Visualisation of a two-dimensional slice of the magnetic (top) and velocity (bottom) fields in the AHFa (left), NDa (middle) and SFa (right) cases.

representative of the general structure of the fields throughout the steady state time frame. The Reynolds numbers are moderately separated: $Re = 742, 994$ and 1190 respectively, but the fields do not obviously differ greatly and exhibit the same level of detail in the small scales. These visualisations demonstrate that, although the forces have very different functional forms, the physical appearance of the fields is similar. Overall we see that all three forces are capable of producing physically-alike steady state behaviour in the same time frame.

B. Comparison of energy and cross helicity spectra

Having identified the onset of the statistically steady state, we can examine the time-averaged energy spectra (Fig. 3). The spectra coincide in a small inertial subrange but spread out slightly at the large and small scales. It is worth bearing in mind that the Reynolds numbers of these systems do differ, with AHF being the smallest and SF the largest, but that the dissipation (and therefore the energy injected) are similar. All of our simulations had the same low- k behaviour, with the ND and SF runs having a peak at $k = 1$ and the AHF types peaking at $k = 2$.

Most of our simulations show a steep k^{-2} power law scaling for the kinetic energy and possibly a small range in which the magnetic energy follows a similar scaling. This scaling is characteristic of the weak turbulence regime, in which Alfvén waves travel along the field lines of a guiding magnetic field and collide more than they cascade [38, 39]. The presence of this scaling could indicate that

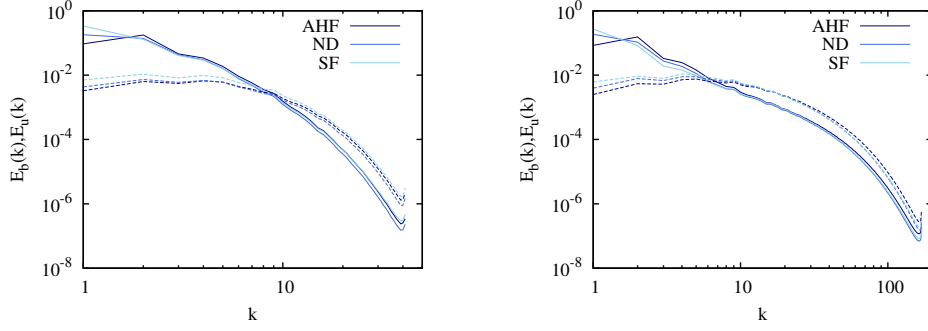


FIG. 3: Spectra of kinetic energy (solid lines) and magnetic energy (dashed lines) for runs AHFf, NDf, SFf (left) and AHFa, NDa, SFa (right).

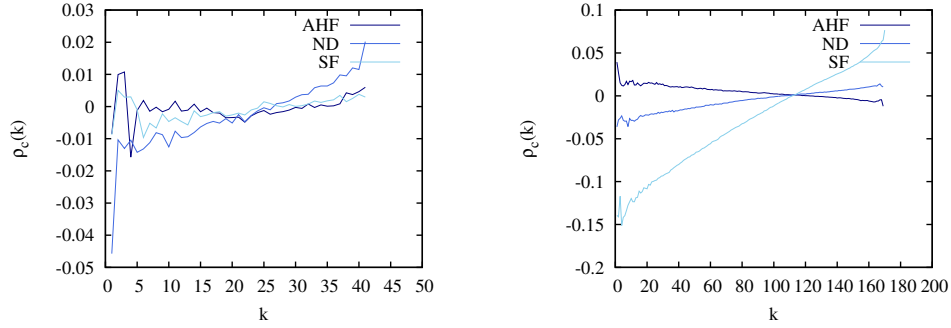


FIG. 4: Spectra of relative cross helicity for runs AHFf, NDf, SFf (left) and AHFa, NDa, SFa (right).

the fields are not fully isotropic.

The small kinks in the spectra, particularly noticable at $k = 3, 9$ and 15 , are numerical artefacts. The reason is as follows. The density of states of wavevectors with magnitude k is $4\pi k^2$. Since our turbulence is generated on a discrete Cartesian lattice, most points do not have integer values of k and so a shell-average of points with wavenumbers $n - 0.5 \leq k < n + 0.5$ is used when calculating spectral quantities. This means that sometimes the density of states in a particular shell will be higher or lower than the continuum limit and so bumps appear in the energy spectra.

The magnetic and kinetic helicity generally remained negligible (see Tab. I), however some simulations developed a build-up of cross helicity, for example SFa which had a time-averaged (normalised) value of $\rho_c = -0.156$. In simulations such as that one, we can see that the cross helicity spectrum is peaked at the forcing scales (as shown in Fig. 4) and therefore conclude that it has been injected by the forcing function. There also tends to be a build-up in the normalised cross helicity at small scales but that is not relevant, as the energy is contained in the

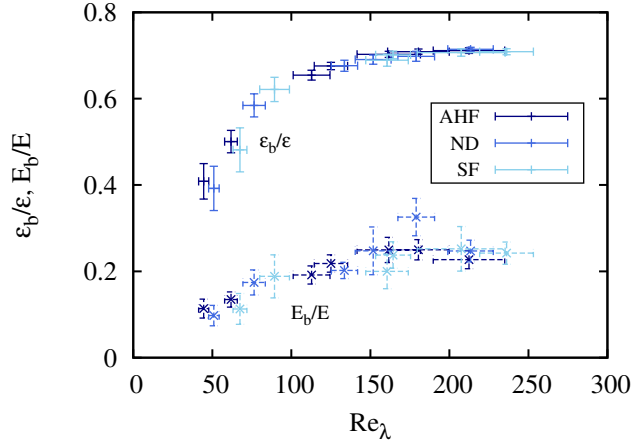


FIG. 5: Fraction of magnetic dissipation ϵ_b/ϵ (plusses) and magnetic energy E_b/E (crosses) as a function of Taylor Reynolds number.

large scales. Although the magnetic helicity fluctuations are small, as expected, the growth of cross helicity is more surprising. It is generally assumed that cross helicity enters the system through the alignment of a kinetic force and a magnetic force in Fourier space, however it actually enters through the alignment of the kinetic force with the magnetic field (and, when present, the magnetic force with the velocity field).

C. Energy and dissipation ratios

In our tests, only the velocity field was forced and so the magnetic field was sustained through the transfer of kinetic to magnetic energy, that is, dynamo action. It is useful to know how efficient the system is at sustaining its magnetic field, which had initial conditions such that it was in equipartition with the velocity field at $t = 0$. Figure 5 shows the ratios E_b/E and ϵ_b/ϵ as a function of Taylor-scale Reynolds number. The Taylor-scale Reynolds number is used instead of the integral-scale Reynolds number because we are interested in comparing the effects of the forces at smaller scales than the forcing range. The measurements of E_b/E and ϵ_b/ϵ follow a clear trend regardless of the way in which the turbulence was forced. In particular, the magnetic dissipation fraction asymptotes quickly to $\epsilon_b/\epsilon \sim 0.71$. This is in agreement with other results for nonhelical simulations with unity magnetic Prandtl number [34, 40]. The magnetic energy fraction displays slightly more erratic behaviour, particularly in run ND. The scatter is expected because the energy is dominated by the more volatile forcing scales, while the dissipation takes place at small scales. We conclude that the energy transfer and

dissipation produced by each type of force is consistent.

D. Conservation of ideal invariants

The total energy, magnetic helicity and cross helicity are conserved in the ideal (non-dissipative) limit. It is therefore desirable for the helicities to remain approximately constant during a statistically steady state. The total energy in the system fluctuates around a constant value as energy is injected and dissipated and we expect the same from the other two ideal invariants. The initial conditions in our simulations have zero magnetic and cross helicity. The time evolution of relative magnetic helicity and cross helicity is shown in Fig. 6. The magnetic helicity remains very close to zero in all cases: the average value is within one standard deviation of zero in all our simulations, irrespective of the chosen forcing method. This could be expected since the magnetic field is not directly forced and should therefore be less susceptible to large variations.

The cross helicity, on the other hand, is not so well conserved in some cases, with large fluctuations away from zero lasting for long times. This is particularly prevalent in the ND and SF runs, with fluctuations up to $\rho_c \simeq 0.3$ at times. Since ND feeds the velocity field back into itself, small fluctuations in cross helicity could be amplified, leading to a runaway effect at large scales. In Fig. 4 we saw that the relative cross helicity is peaked at the forcing scales, so it is clear that the growth of cross helicity is from the forcing. To guarantee negligible injection of cross helicity, the alignment between \mathbf{f} and \mathbf{b} in Fourier space (and when a magnetic force \mathbf{f}_b is present, the alignment between \mathbf{f}_b and \mathbf{u}) should remain negligible. The unusually large fraction of magnetic energy in Run NDb, as seen in Fig. 5, could be connected to the presence of cross helicity.

The influence of intermediate values of cross helicity is not well understood, although it is known that systems with nonzero cross helicity can tend towards an Alfvénic state in which the cross helicity is maximal [41]. One of the findings of this study which has not been anticipated in the literature is that helicity can unexpectedly enter the system through certain forcing functions. Thus it is of practical importance to monitor and control its injection.

E. Comparison of repeated simulations

Generally when using DNS we make the assumption of ergodicity, that is, that in stationary turbulence the time-averaged values from one simulation are equivalent to ensemble-averaged values where the ensemble consists of many simulations. Thus for any set of parameters, usually only one simulation is performed and statistics are obtained by averaging over snapshots in time once the system has reached a steady state. This is the approach we took in the preceding section. However,

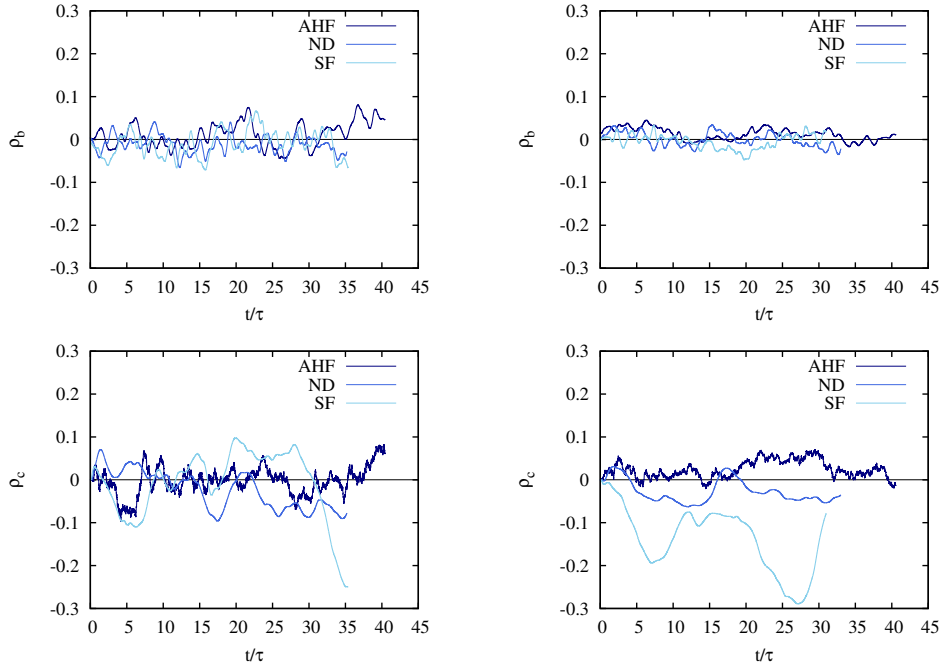


FIG. 6: Evolution of relative magnetic helicity (top) and relative cross helicity (bottom) for runs AHFf, NDf, SFf (left) and AHFa, NDa, SFa (right). τ is the time-averaged large eddy turnover time. Note that the y-axis extends to ± 0.3 but the maximum possible values are 1.

we found significant variations in cross helicity over time which prompted us to question how valid the ergodic principle is in situations where the injection of helicities cannot be controlled. Furthermore, one might expect that the fluctuations of the ideal invariants would decrease as we increase the Reynolds number, since we are increasing the number of interactions at each length scale, but this does not seem to be the case in our tests. Large fluctuations in cross helicity alter the behaviour of a flow, for example in Run NDf, which had an average relative cross helicity $\rho_c = 0.212$ and a larger than expected energy fraction E_b/E . On the other hand, the physical appearance of the fields does not seem to be strongly affected by moderate amounts of relative cross-helicity, as can be seen in Fig. 2, in which the relative cross helicity at the time of measurement for each run (AHFa, NDa and SFa) was $\rho_c = 0.06, -0.02, -0.21$ respectively.

To test the variability of the cross helicity and its effect on the distribution of energy between the two fields, we ran an ensemble of 20 simulations for each forcing type on a 128^3 grid using the same parameters as the AHFf, NDf and SFf runs but with different initial conditions. The time-averaged Reynolds numbers and relative cross helicity are shown in Tab. II. In all cases, the time-averaged Reynolds numbers stayed in a close range. The relative cross helicity, however, was less

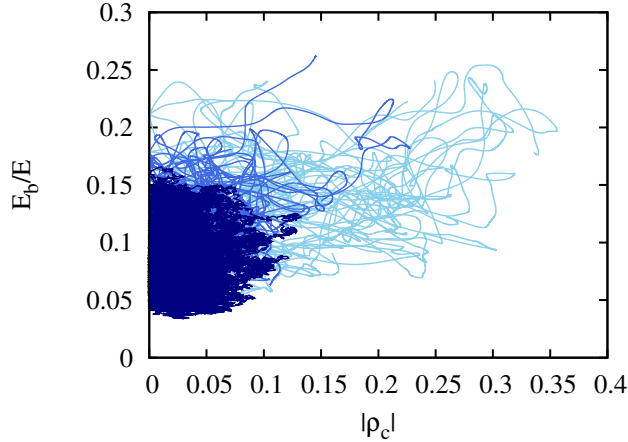


FIG. 7: Magnitude of relative cross helicity versus the fraction of magnetic energy E_b/E at each point in time of the steady-state ensembles for AHF (dark), ND (medium), SF (light).

Type	Re	Re_λ	$ \rho_c $	#
AHF	80 – 87	44 – 46	$7.41 \times 10^{-6} - 0.0256$	20
ND	100 – 111	52 – 57	0.000686 – 0.0561	20
SF	132 – 141	66 – 70	0.00111 – 0.193	20
SF512	129 – 135	64 – 66	0.0447 – 0.127	3

TABLE II: The range of time-averaged quantities (integral-scale Reynolds number Re, Taylor-scale Reynolds number Re_λ and relative cross helicity magnitude $|\rho_c|$) from ensembles of each of the three forcing types with $\nu = 0.008$.

The final row shows data from a small ensemble of runs equivalent to SF but with a higher resolution.

consistent, particularly in the SF ensembles. We plotted the time evolution of the magnetic energy fraction against the relative cross helicity for all our simulations to explore the possibility of a connection between the two quantities (Fig. 7). We see further evidence of the variability of cross helicity in the SF cases and also what seems to be a tendency for the magnetic energy fraction to increase as the magnitude of cross helicity increases.

An explanation of the poor conservation of cross helicity in the case of sinusoidal forcing could be to do with the discretisation of the lattice, as mentioned in Sec. II C. The number of grid points was increased with the Reynolds number to maintain good resolution, however for the sake of consistency we ran an additional three realisations of the SF type with $\nu = 0.008$ using a box with $N = 512$

(compared to the original $N = 128$). We found the same large fluctuations even in these runs and so can rule out discretisation effects as the primary cause.

The results of this section suggest that the ergodic principle does not hold well when the fluid is subject to our sinusoidal forcing, as the relative cross helicity can vary significantly from one run to another, which affects aspects of the system such as the energy distribution. This is also likely the case with ND to a lesser degree. The concept of nonuniversality is of interest here, since two simulations with large average values of cross helicity of opposite sign would surely not behave in the same way as a system with zero cross helicity, despite the ensemble-averaged values being small. So perhaps the solution is simply to monitor the ideal invariants carefully and be wary of large variations. Nevertheless, the AHF reliably maintains small values of cross helicity and so these extra considerations are not required.

IV. CONCLUSIONS

In this paper we explored the similarities and differences of three different types of kinetic forcing function in homogeneous, incompressible magnetohydrodynamic simulations without a mean magnetic field. In particular, we looked at negative damping, a random adjustable helicity forcing in which the kinetic helicity input was set to zero, and a nonhelical deterministic sinusoidal forcing. From a practical point of view, the AHF was least effective at reaching large Reynolds numbers at a given resolution but most effective at maintaining small values of cross helicity. This is presumably because of the random nature of the force. It also produced slightly different energy spectra at small wavenumbers compared to the other two forcing types. We found that all three forces produce a steady state in a similar amount of simulation time, with reasonable agreement of dynamo efficiency, interpreted via the energy and dissipation fractions.

We considered the fluctuations of energy, relative magnetic helicity and relative cross helicity over time since these three quantities are the ideal invariants in MHD. The magnetic helicity was well-conserved in all three cases, with only very small fluctuations, whereas the cross helicity was more erratic. In some simulations - particularly the ND and SF types - the cross helicity had large, long-term deviations from zero, although the deviations were not large enough to cause the system to become fully Alfvénic. However, it led us to question the validity of ergodicity when using forcing functions which are prone to causing build-ups in cross helicity, since large variations of cross helicity influence the development of the flow. We found that there may be a tendency for the magnetic energy fraction to increase as the relative cross helicity increases, but the cross helicity fluctuations were not large enough to be able to say this definitively. It is important to make sure that the rate of injection of cross helicity $\langle \mathbf{f} \cdot \mathbf{b} \rangle$ is small. This analysis has highlighted some of the subtle problems with the control of ideal invariants

in forced turbulence. Future work could involve carrying out more simulations with higher Reynolds numbers to further assess the effect on fluctuations of the ideal invariants. The AHF simulations had the best conservation of cross helicity, presumably due to the stochastic nature of the force. Adding a random phase to the SF function might therefore help to minimise the cross helicity input. It would also be interesting to study flows which are forced magnetically (with or without kinetic forcing).

While we cannot make any definite statements about the equivalence of all forcing functions at large Reynolds numbers, we have at least confirmed that three different implementations, typical of the kind generally used in MHD simulations, produce flows with similar characteristics, albeit with fairly significant deviations at the forcing scales. Forcing functions which do not control the injection of helicities should be monitored carefully. However, in the case of kinetic-only forcing which we have focussed on, discrepancies introduced by different forcing functions have not been too large. Thus, provided that the level of ideal invariants is maintained, it seems safe to rely on the hypothesis that the small-scale behaviour of a system is independent of how it is forced, at least in the case of kinetically-forced, homogeneous, nonhelical magnetohydrodynamics.

ACKNOWLEDGMENTS

This work used the ARCHER UK National Supercomputing Service [42]. AB acknowledges funding from the Science and Technology Facilities Council and MEM from the Engineering and Physical Sciences Research Council (EP/M506515/1). MFL acknowledges funding from the European Research Council under the European Unions Seventh Framework Programme, ERC Grant Agreement No 339032. The data is publicly available online[43].

-
- [1] D. Biskamp. *Magnetohydrodynamic Turbulence*. Cambridge University Press, Cambridge, UK, 2003.
 - [2] P. A. Davidson. *An Introduction to Magnetohydrodynamics*. Cambridge University Press, 2001.
 - [3] U. Frisch. *Turbulence: The Legacy of A. N. Kolmogorov*. Cambridge University Press, Cambridge, UK, 1995.
 - [4] M. K. Verma. Statistical theory of magnetohydrodynamic turbulence: recent results. *Physics Reports*, 401(5-6):229–380, 2004.
 - [5] V. Eswaran and S. B. Pope. An examination of forcing in direct numerical simulations of turbulence. *Computers & Fluids*, 16(3):257–278, 1988.

- [6] K. Alvelius. Random forcing of three-dimensional homogeneous turbulence. *Physics of Fluids*, 11(7):1880–1889, 1999.
- [7] Z. Zeren and B. Bédard. Spectral and physical forcing of turbulence. In *Progress in Turbulence III: Proceedings of the iTi Conference in Turbulence 2008*, pages 9–12. Springer Berlin Heidelberg, 2010.
- [8] W. D. McComb. *Homogeneous, Isotropic Turbulence: Phenomenology, Renormalization and Statistical Closures*. Oxford Science Publications, Oxford, UK, 2014.
- [9] G. K. Batchelor. *The Theory of Homogeneous Turbulence*. Cambridge University Press, Cambridge, UK, 1953.
- [10] J. Léorat, U. Frisch, and A. Pouquet. Helical magnetohydrodynamic turbulence and the nonlinear dynamo problem. *Annals of the New York Academy of Sciences*, 257(1):173–176, 1975.
- [11] A. Pouquet, U. Frisch, and J. Léorat. Strong MHD helical turbulence and the nonlinear dynamo effect. *J. Fluid Mech.*, 77:321–354, 1976.
- [12] A. Alexakis, P. D. Mininni, and A. Pouquet. On the inverse cascade of magnetic helicity. *Astrophys. J.*, 640:335–343, 2006.
- [13] A. Alexakis, P. D. Mininni, and A. Pouquet. Turbulent cascades, transfer, and scale interactions in magnetohydrodynamics. *New Journal of Physics*, 9:298, 2007.
- [14] H. K. Moffat. The degree of knottedness of tangled vortex lines. *J. Fluid Mech.*, 35:117–129, 1969.
- [15] M. F. Linkmann, A. Berera, W. D. McComb, and M. E. McKay. Nonuniversality and finite dissipation in decaying magnetohydrodynamic turbulence. *Phys. Rev. Lett.*, 114:235001, Jun 2015.
- [16] M. Linkmann, A. Berera, and E. E. Goldstraw. Reynolds-number dependence of the dimensionless dissipation rate in homogeneous magnetohydrodynamic turbulence. *Phys. Rev. E*, 95:013102, Jan 2017.
- [17] V. Dallas and A. Alexakis. The signature of initial conditions of magnetohydrodynamic turbulence. *Astrophys. J.*, 788(2):L36, 2014.
- [18] M. Dobrowolny, A. Mangeney, and P. Veltri. Fully developed anisotropic hydromagnetic turbulence in interplanetary space. *Phys. Rev. Lett.*, 45:144–147, Jul 1980.
- [19] T. Stribling and W. H. Matthaeus. Relaxation processes in a low-order three-dimensional magnetohydrodynamics model. *Physics of Fluids B: Plasma Physics*, 3(8):1848–1864, 1991.
- [20] V. Dallas and A. Alexakis. Self-organisation and non-linear dynamics in driven magnetohydrodynamic turbulent flows. *Physics of Fluids*, 27(4), 2015.
- [21] S. R. Yoffe. *Investigation of the transfer and dissipation of energy in isotropic turbulence*. PhD thesis, The University of Edinburgh, Scotland, 2012.
- [22] M. F. Linkmann. *Self-organisation processes in (magneto)hydrodynamic turbulence*. PhD thesis, The University of Edinburgh, Scotland, 2016.
- [23] L. Machiels. Predictability of small-scale motion in isotropic fluid turbulence. *Phys. Rev. Lett.*, 79:3411–3414, 1997.

- [24] J. Jiménez, A. A. Wray, P. G. Saffman, and R. S. Rogallo. The structure of intense vorticity in isotropic turbulence. *Journal of Fluid Mechanics*, 255:6590, 1993.
- [25] Y. Kaneda, T. Ishihara, M. Yokokawa, K. Itakura, and A. Uno. Energy dissipation rate and energy spectrum in high resolution direct numerical simulations of turbulence in a periodic box. *Physics of Fluids*, 15(2):L21–L24, 2003.
- [26] Y. Kaneda and T. Ishihara. High-resolution direct numerical simulation of turbulence. *Journal of Turbulence*, 7:N20, 2006.
- [27] G. Sahoo, P. Perlekar, and R. Pandit. Systematics of the magnetic-Prandtl-number dependence of homogeneous, isotropic magnetohydrodynamic turbulence. *New Journal of Physics*, 13(1):013036, 2011.
- [28] W. D. McComb, M. F. Linkmann, A. Berera, S. R. Yoffe, and B. Jankauskas. Self-organization and transition to turbulence in isotropic fluid motion driven by negative damping at low wavenumbers. *Journal of Physics A: Mathematical and Theoretical*, 48(25):25FT01, 2015.
- [29] M. F. Linkmann and A. Morozov. Sudden relaminarization and lifetimes in forced isotropic turbulence. *Phys. Rev. Lett.*, 115:134502, Sep 2015.
- [30] A. Brandenburg. The inverse cascade and nonlinear alpha-effect in simulations of isotropic helical hydromagnetic turbulence. *The Astrophysical Journal*, 550(2):824, 2001.
- [31] S. K. Malapaka and W.-C. Müller. Large-scale magnetic structure formation in three-dimensional magnetohydrodynamic turbulence. *The Astrophysical Journal*, 778(1):21, 2013.
- [32] W. C. Müller, S. K. Malapaka, and A. Busse. Inverse cascade of magnetic helicity in magnetohydrodynamic turbulence. *Phys. Rev. E.*, 85:015302, 2012.
- [33] L. Biferale, S. Musacchio, and F. Toschi. Inverse energy cascade in three-dimensional isotropic turbulence. *Phys. Rev. Lett.*, 108:164501, Apr 2012.
- [34] A. Brandenburg. Magnetic Prandtl number dependence of the kinetic-to-magnetic dissipation ratio. *The Astrophysical Journal*, 791(1):12, 2014.
- [35] B. Galanti, P. L. Sulem, and A. Pouquet. Linear and non-linear dynamos associated with ABC flows. *Geophysical & Astrophysical Fluid Dynamics*, 66(1-4):183–208, 1992.
- [36] D. Galloway. ABC flows then and now. *Geophysical & Astrophysical Fluid Dynamics*, 106(4-5):450–467, 2012.
- [37] P. D. Mininni. Inverse cascades and α effect at a low magnetic Prandtl number. *Phys. Rev. E*, 76:026316, Aug 2007.
- [38] J. C. Perez and S. Boldyrev. On weak and strong magnetohydrodynamic turbulence. *The Astrophysical Journal Letters*, 672(1):L61, 2008.
- [39] Y. Lithwick and P. Goldreich. Imbalanced weak magnetohydrodynamic turbulence. *The Astrophysical Journal*, 582(2):1220, 2003.
- [40] N. E. L. Haugen, A. Brandenburg, and W. Dobler. Is nonhelical hydromagnetic turbulence peaked at small scales? *The Astrophysical Journal Letters*, 597(2):L141,

2003.

- [41] R. Grappin, J. Léorat, and A. Pouquet. Dependence of MHD turbulence spectra on the velocity field-magnetic field correlation. *Astronomy and Astrophysics*, 126(1):51–58, 1983.
- [42] <http://www.archer.ac.uk/>.
- [43] <http://dx.doi.org/10.7488/ds/1999>.